A rigid elliptical cross-sectional projectile with different geometrical characteristics penetration into concrete target

Xianghui Dai*, Kehui Wang, Jian Duan, Mingrui Li, Bingwen Qian, Gang Zhou

Laboratory of Intense Dynamic Loading and Effect,

Northwest Institute of Nuclear Technology,

Xi'an, Shaanxi 710024, P R China

E-mail: dxh19860715@163.com

Introduction

The elliptical cross-sectional projectile can adapt well to the flat "wave-passing body" shape of the hypersonic weapon and increase the payload of the weapon platform. However, the penetration performance of elliptical cross-sectional projectiles into concrete targets is still not fully understood. In the present study, general geometry functions are introduced to define the geometrical characteristics of four types of elliptical cross-sectional projectiles, theoretical models for deep penetration of these projectiles into concrete targets are developed. The deceleration, velocity, and displacement of the projectiles during the penetration process are then obtained based on the present models, and comparative analysis of the penetration performance of these projectiles is conducted.

Theoretical model

Nose surface geometry functions of elliptical cross-sectional projectiles

General geometry functions are introduced to define the geometrical characteristics of four types of elliptical cross-sectional projectiles.

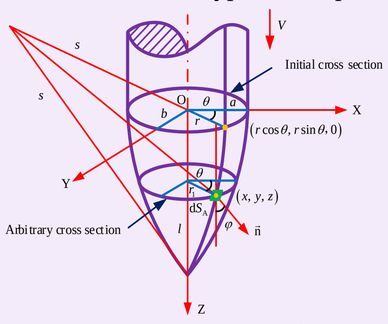

Figure 1. Ogive-nose projectile.

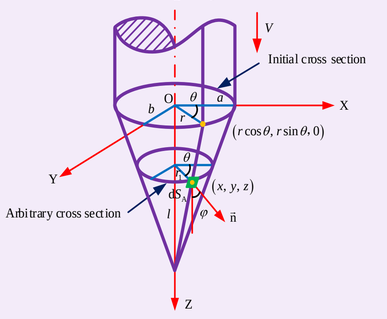

Figure 2. Conical-nose projectile.

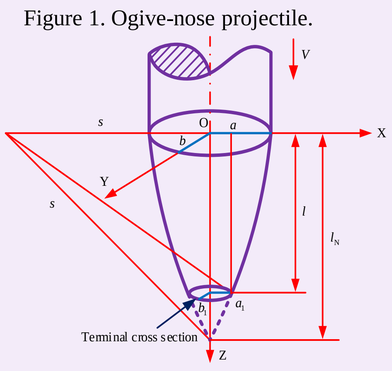

Figure 3. Truncated-ogive-nose projectile.

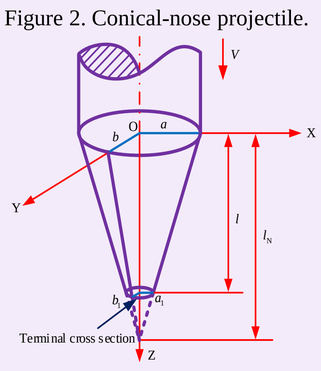

Figure 4. Truncated-conical-nose projectile.

Ogive-nose and truncated-ogive-nose projectiles:

$$f(x,y,z)=x^2+y^2+z^2+\frac{l^2\sqrt{(bx)^2+(ay)^2}}{ab}-\frac{ab(x^2+y^2)}{\sqrt{(bx)^2+(ay)^2}}-l^2=0$$

Conical-nose and truncated-conical-nose projectiles:

$$f(x,y,z)=\left(\frac{\sqrt{b^2x^2+a^2y^2}}{ab}-1\right)l+z=0$$

Resistance of the elliptical cross-sectional projectiles

According to the spherical dynamic cavity-expansion theory [1], and integrating the normal stress on the projectile nose to obtain the axial resistance:

$$F_z=A+BV^2$$

where A and B are the static resistance and dynamic resistance coefficient of ogive-nose projectile, respectively, which have similar expressions for the other three projectiles.

$$A=Rab\int_0^{2\pi}\int_0^1\frac{2(1-\rho)^{1/2}l_1}{\left\{\frac{\cos^2\alpha\left[2a^2(\rho-1)+l_1^2\right]^2}{a^2}+\frac{\sin^2\alpha\left[2b^2(\rho-1)+l_1^2\right]^2}{b^2}+4(1-\rho)l_1^2\right\}^{1/2}}\times\left\{1+\frac{1}{4(1-\rho)l_1^2}\left[\frac{\cos^2\alpha\left[2a^2(\rho-1)+l_1^2\right]^2}{a^2}+\frac{\sin^2\alpha\left[2b^2(\rho-1)+l_1^2\right]^2}{b^2}\right]\right\}^{1/2}\rho\,d\rho\,d\alpha$$

$$B=\rho_t ab\int_0^{2\pi}\int_0^1\frac{8(1-\rho)^{3/2}l_1^3}{\left\{\frac{\cos^2\alpha\left[2a^2(\rho-1)+l_1^2\right]^2}{a^2}+\frac{\sin^2\alpha\left[2b^2(\rho-1)+l_1^2\right]^2}{b^2}+4(1-\rho)l_1^2\right\}^{3/2}}\times\left\{1+\frac{1}{4(1-\rho)l_1^2}\left[\frac{\cos^2\alpha\left[2a^2(\rho-1)+l_1^2\right]^2}{a^2}+\frac{\sin^2\alpha\left[2b^2(\rho-1)+l_1^2\right]^2}{b^2}\right]\right\}^{1/2}\rho\,d\rho\,d\alpha$$

Penetration process

The two-stage penetration model is also utilized for the elliptical cross-sectional projectile [2].

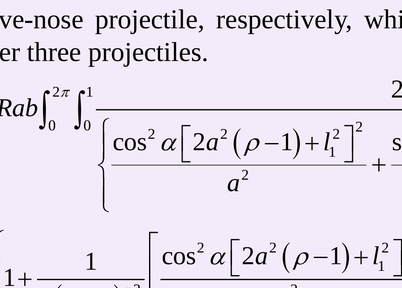

Figure 5. Schematic of normal penetration of concrete target by an elliptical cross-sectional projectile.

Based on the Newton's second law, the final penetration depth is given by

$$H^*=\frac{m}{2B}\ln\left(1+\frac{BV_1^2}{A}\right)+kd$$

$$V_1=\left(\frac{V_0^2-Akd/m}{1+Bkd/m}\right)^{1/2}$$

Validation

Nose surface geometry functions

According to the nose surface geometry, the nose shapes of the elliptical cross-sectional projectiles are accurately drawn, which indicate that the nose surface geometry functions and geometric modeling process are correct.

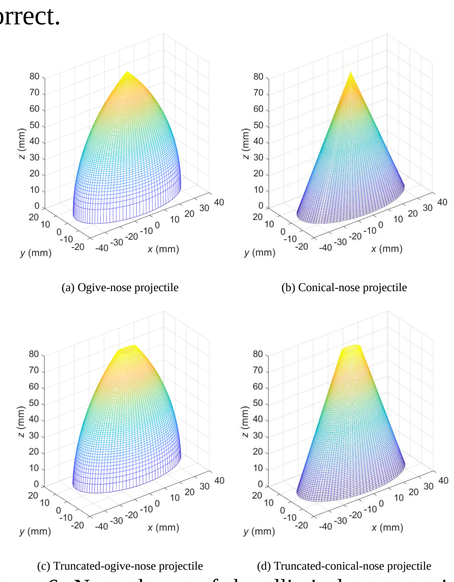

(a) Ogive-nose projectile (b) Conical-nose projectile

(c) Truncated-ogive-nose projectile (d) Truncated-conical-nose projectile

Figure 6. Nose shapes of the elliptical cross-sectional projectiles.

Penetration depth predictions of the circular cross-sectional projectiles

When $a = b$, the elliptical cross-sectional projectile degenerates into a circular cross-sectional projectile. The penetration depth predictions of the present models are consistent with that of the semi-empirical formulae.

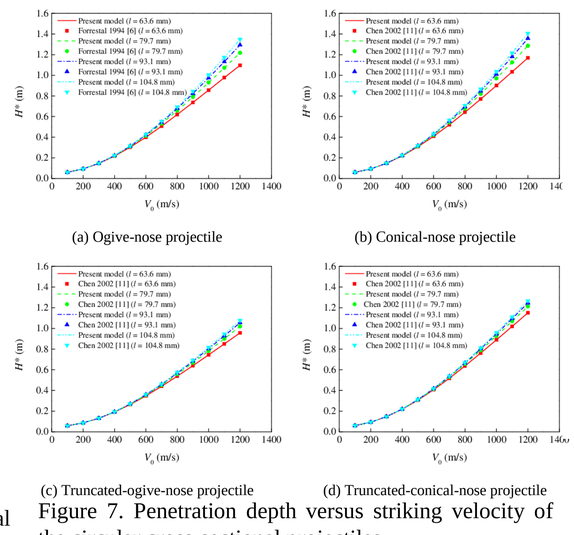

(a) Ogive-nose projectile (b) Conical-nose projectile

(c) Truncated-ogive-nose projectile (d) Truncated-conical-nose projectile

Figure 7. Penetration depth versus striking velocity of the circular cross-sectional projectiles.

Experimental analyses

The penetration depth predictions agree well with the test data, and the maximum deviation is 15.8%. Although significant differences exist between the projectiles and striking velocities, the model predictions are in good agreement with the test data.

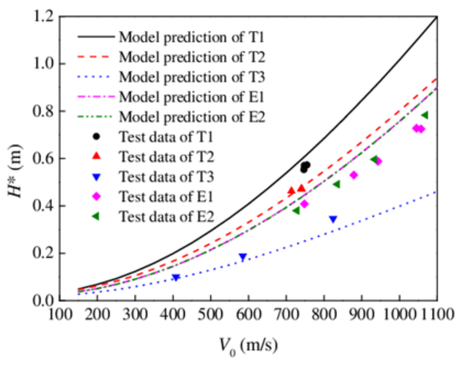

Figure 8. Test data and model predictions of the elliptical cross-sectional ogive-nose projectiles.

Results and Discussion

Projectile motion prediction

The deceleration, velocity, and displacement of four types of elliptical cross-sectional projectiles during the penetration process are calculated.

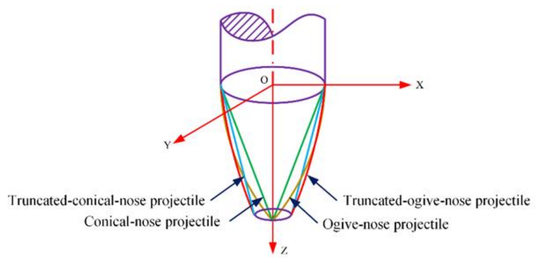

Figure 9. Side outline of the four types of elliptical cross-sectional projectiles.

The tendency of the deceleration–time, velocity–time, and displacement–time curves of four types of elliptical cross-sectional projectiles are similar, and the differences lie in the deceleration amplitude, penetration time, and penetration depth. When the nose length is sufficiently large, the conical-nose elliptical cross-sectional projectile tends to be subjected to lower deceleration, exhibits a slower drop in velocity during the penetration process, and achieves the deepest penetration depth.

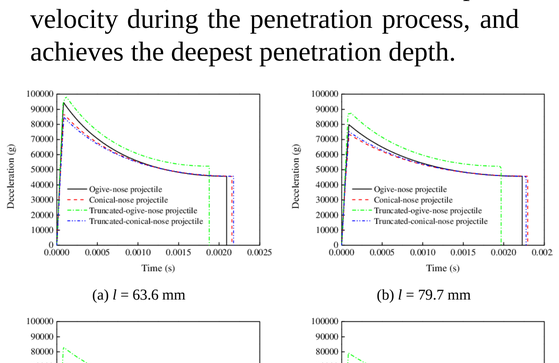

(a) l = 63.6 mm (b) l = 79.7 mm

(c) l = 93.1 mm (d) l = 104.8 mm

Figure 10. Deceleration versus time of various elliptical cross-sectional projectiles.

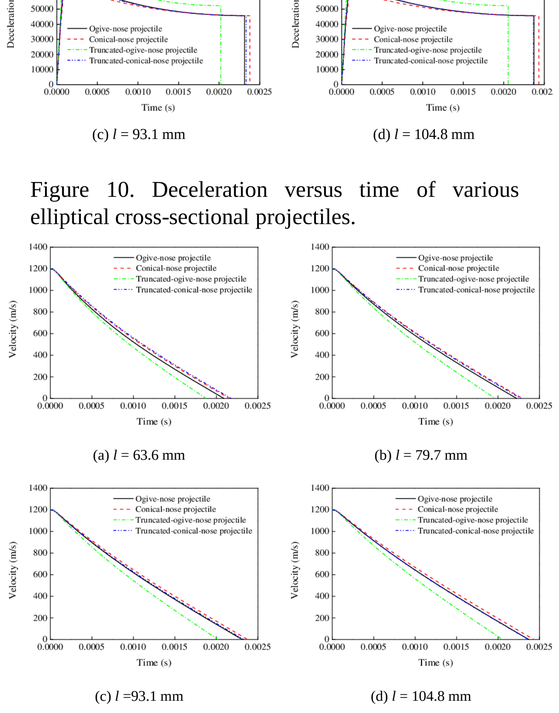

(a) l = 63.6 mm (b) l = 79.7 mm

(c) l =93.1 mm (d) l = 104.8 mm

Figure 11. Velocity versus time of various elliptical cross-sectional projectiles.

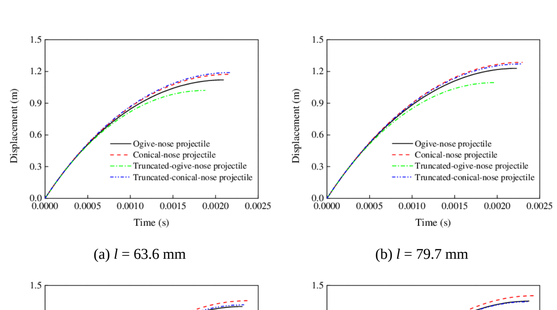

(a) l = 63.6 mm (b) l = 79.7 mm

(c) l = 93.1 mm (d) l = 104.8 mm

Figure 12. Displacement versus time of various elliptical cross-sectional projectiles.

Figures 10–12 show that the deceleration–time, velocity–time, and displacement–time curves of the ogive-nose and truncated-conical-nose projectiles are almost coincident when l = 104.8 m.

Penetration performance

The conical-nose projectile achieves the deepest penetration depth, followed by the truncated-conical-nose projectile, the ogive-nose projectile, and finally the truncated-ogive-nose projectile. However, when l = 63.6 mm, the penetration depth of the truncated-conical-nose projectile is slightly larger than that of the conical-nose projectile. Moreover, as the nose length increases, the penetration depth of the ogive-nose projectile gradually approaches or even exceeds that of the truncated-conical-nose projectile.

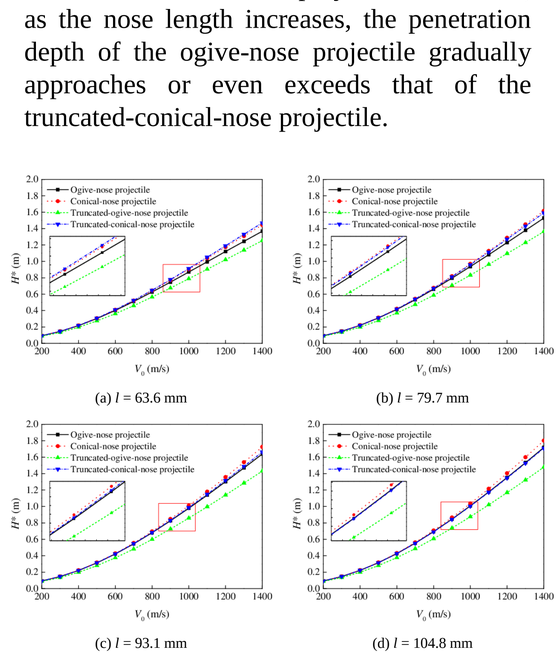

(a) l = 63.6 mm (b) l = 79.7 mm

(c) l = 93.1 mm (d) l = 104.8 mm

Figure 13. Penetration depth versus striking velocity of various elliptical cross-sectional projectiles.

Conclusion

Theoretical models of a rigid elliptical cross-section projectile with different geometrical characteristics penetration into a semi-infinite concrete target are presented based on the dynamic cavity-expansion theory. Moreover, comparative analysis of the motion and penetration performance for four types of elliptical cross-section projectiles is conducted based on the present models. The following main conclusions are drawn:

(1) The penetration equations of four types of elliptical cross-sectional projectiles are in closed form and depend on the striking velocity, geometry, projectile mass, and material properties of the concrete target.

(2) The present model is validated by comparing the predicted penetration depths with the test data for elliptical cross-sectional ogive-nose projectiles, and the maximum deviation is 15.8%.

(3) When the nose length is sufficiently large, the conical-nose elliptical cross-sectional projectile tends to be subjected to lower deceleration, exhibits a slower drop in velocity during the penetration process, and achieves the deepest penetration depth.

(4) The conical-nose elliptical cross-sectional projectile achieves the best penetration performance than the other three types of elliptical cross-sectional projectiles if the nose length is sufficiently large, and the penetration performance of the ogive-nose elliptical cross-sectional projectile gradually approaches or even exceeds that of the truncated-conical-nose elliptical cross-sectional projectile with the increase in the nose length.

Future Efforts:

To further verify the present models, more systematic penetration experiments for a 1.8-kg elliptical cross-sectional projectile with different geometrical characteristics are urgently needed, and this will be the focus of our future study.

Acknowledgments

This work was supported by the National Natural Science Foundation of China (Nos. 11772269, 11802248, and 11872318). The authors would like to thank Prof. Yunliang Li, Mr. Zhiqiang Chen, and Mr. Zikan Shen for their technical support.

References:

[1] Forrestal M, Altman B, and Cargile J. 1994. "An empirical equation for penetration depth of ogive-nose projectiles into concrete targets," Int J Impact Eng., 15(4):395-405.

[2] Li Q, and Chen X. 2003. "Dimensionless formulae for penetration depth of concrete target impacted by a rigid projectile," Int J Impact Eng., 28(1):93-116.

[3] Wang W, Zhang X, Deng J, Zheng Y and Liu C 2018. "Analysis of projectile penetrating into mortar target with elliptical cross-section," Explosive Shock Waves., 38:164-73.

[4] Dong H, Liu Z, Wu H, Gao X, Pi A and Huang F 2019. "Study on penetration characteristics of high-speed elliptical cross-sectional projectiles into concrete," Int J Impact Eng., 132:1-12.